PCCP

Accepted Manuscript

ROYAL SOCIETY OF CHEMISTRY

www.rsc.org/pccp

PCCP

RSCPublishing

PAPER

Controllable growth of durable superhydrophobic coating on copper substrate via electrodeposition

Cite this:
Phys.Chem.Chem.Phys.,*2015*,00, 00000

Ge He[a], Shixiang Lu[*a,b], Wenguo Xu[a], Sabine Szunerits[b], Rabah Boukherroub[b], Haifeng Zhang[a]

Received 00th 00 2015,
Accepted 00th 00 2015

DOI: 10.1039/x0xx00000x

www.rsc.org/

The superhydrophobic coatings on copper substrate are grown *via* electrodeposition followed by thermal annealing. The influence of the deposition potential, zinc ion concentration, deposition time, annealing temperature and annealing time on the wetting properties was systematically investigated. The coating electrodeposited at -1.35 V for 25 min and annealed at 190 ℃ for 60 min exhibited excellent superhydrophobicity with a contact angle as high as 170±2 ° and a sliding angle of almost 0 °. The water drop can fully bounce as a balloon when impinging such a solid surface, exhibiting excellent non-sticking property. By adopting various characterization methods, it was demonstrated that the as-prepared superhydrophobic surfaces also exhibited properties of anticorrosion, antiabrasion, long-term stability and durability and large buoyancy force, which offer an effective strategy and promising industrial applications for fabricating superhydrophobic surfaces on various metallic materials.

1 Introduction

As a widely used engineering material, copper is attractive for its high electrical and thermal conductivity, malleability and mechanical workability. However, copper is susceptible to corrosion, particularly in the presence of aggressive chloride anions.[1] Like any other metal, copper can develop a thin oxide layer on its surface, which can protect it from further corrosion. However, recent results showed that the most durable protection against corrosion is obtained by the formation of multilayer superhydrophobic coatings in combination with oxide layer.[2-5] Superhydrophobic coatings form an important and successful barrier to slow down the breaking of the oxide layer and thus prevent the surface underneath from further corrosion.[6] Luckily, copper-based surfaces are quite easily rendered superhydrophobic. Much research work has been conducted on the superhydrophobic properties of Cu-based surfaces, such as CuO micro-cabbages on Cu foil,[7] $Cu(OH)_2$ nanowires on Cu surfaces,[8] 3D Cu porous films[9] and patterns,[10, 11] copper tubes,[12] etc.

Besides acting as anticorrosion barrier, superhydrophobic surfaces (SHSs) with a water contact angle (WCA) greater than 150 ° and a sliding angle (SA) less than 5 ° have drawn huge attention for both fundamental research and practical applications. Indeed, such surfaces are found in nature (plant surfaces) and display outstanding properties like self-cleaning,[13] anti-icing,[14] oil-water separation,[15] etc. Although the fabrication and application of SHSs is not a new topic, this field always attracts considerable attention. Therefore, many different routes are reported for the production of such surfaces, allowing a vast range of materials to be used as substrates, or modified to give superhydrophobic surfaces.[16-27]

However, some of the preparation methods for making SHSs are potentially costly and time-consuming for industrial implementation, as they require tedious fabrication processes and use of organic reagents. Hereon, on account of the facile, low cost and suitable for industrial applications, electrodeposition is considered as an effective technique for the fabrication of large-area SHSs as well as providing versatility in tailoring the architecture of metals at the micro/nano scale.[28, 29] Furthermore, by varying the metal ion concentrateion and the electrodeposition conditions (electrolyte, deposition methodand charge), both morphology and chemistry of the surface can be modulated, allowing controllable preparation of SHSs.

Generally speaking, artificial SHSs are obtained through the combination of surface roughness and low surface energy coating. Two strategies are usually adopted in order to create a SHS. The first approach consists on the generation of rough surfaces, followed by coating with low surface energy materials. The second strategy relies on roughening the surface of hydrophobic materials.[18, 30-32] Recent studies on lotus and rice leaves revealed that a SHS with both a large WCA and a small SA needs the cooperation of micro- and nanostructures, and the arrangement of the micro/nano structures on this surface can influence the way a water droplet tends to move.[33] Besides, these complex multi-scale structures in which there are nanostructures on the top of microstructures can effectively increase

the surface area and roughness and amplify the solid-liquid contact area. The results from the natural world provide a guide for constructing artificial SHSs and designing surfaces with controllable wettability, since nature does not require the low surface energy of $-CH_3$ groups or fluorocarbons to achieve these effects. This plainly demonstrates that extremely low surface energy coatings are not necessary to achieve non-wetting surfaces,[34] because the modified surfaces may be not stable and may restrain some other properties of materials like heat conduction and electrical conduction due to organic films. Some of us have prepared various superhydrophobic materials with excellent performance on different substrates by adopting chemical replacement deposition method without additional modification with low surface energy materials.[35-38]

In this work, we propose a new approach for the preparation of SHSs on copper substrate without any modification with low surface energy coating using a rapid and mild electrodeposition method. It was achieved by immersion of a copper sheet in an electrolytic buffer solution of zinc ions under amperometric conditions followed by thermal annealing. The whole process is simple and cost-effective. The resulting SHS has the merits of acting as an anti-corrosion barrier and displays anti-abrasion properties. The effects of deposition potential, zinc ion concentration, deposition time, annealing temperature and annealing time on the contact angle were investigated.

2 Experimental Section

2.1 Reagents and materials

Nitric acid (HNO_3, 65%), ammonia ($NH_3 \cdot H_2O$), acetone (CH_3COCH_3, 99.5%), ethanol (C_2H_5OH, 99.5%), potassium chloride (KCl) and zinc acetate [$Zn(CH_3COO)_2 \cdot 2H_2O$] were purchased from China Beijing Fine Chemical Co. Ltd. and used as received without further purification. Copper sheet (99.9%) (2.0 cm×1.0 cm×0.1 cm) were obtained from Beijing Nonferrous Metal Research Institute. The water used was purified through a distillation system.

2.2 Electrochemical fabrication of superhydrophobic coatings on copper substrate

A surface treatment of the copper substrate was conducted to remove organic contaminants and oxide layer from the surface by ultrasonically cleaning sequentially with a mixture of ethanol and acetone (v/v: 1/1) and deionized water for 10 min. Then the samples were set perpendicularly in unplasticized poly vinyl chloride (UPVC) tube and were etched in 2.96 mol L^{-1} HNO_3 solution for 4 min to generate a rough surface, followed by rinsing with a large amount of distilled water and drying at room temperature.

The electrochemical experiments were carried out in a classical three-electrode-cell: a copper sheet acted as working electrode, platinum foil and saturated calomel electrode (SCE) were used as counter electrode and reference electrode, respectively. Cyclic voltammetry (CV) was carried out to determine the reduction potential of the zinc ion before electrochemical deposition of the film in an electrolytic solution. The subacid electrolytic solution consisting of 0.02 mol/L $Zn(CH_3COO)_2$, 0.1 mol/L KCl and 0.017 mol/L $NH_3 \cdot H_2O$ solution was used in the ambient condition without de-aerating; KCl was used as supporting electrolyte to increase the conductivity as well as make the crystal delicate and uniform. And $NH_3 \cdot H_2O$ was used as a ligand combined with Zn^{2+} to change the potential of Zn^{2+} reduction as well as control the PH of the solution. After electrodeposition, the copper sheet was brought out of solution, washed thoroughly with distilled water and dried in air. Soon afterwards, the samples were placed in a Petri dish covered with filter paper[38] and annealed at 190 ℃ for 60 min in the oven in the air. The whole process is illustrated in Scheme 1.

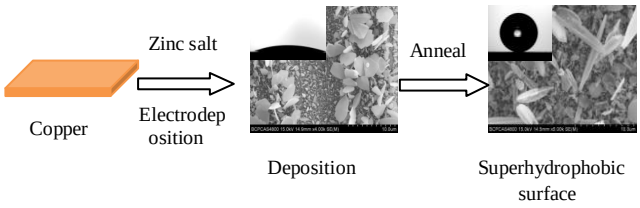

Scheme 1 Illustration of the preparation method of the superhydrophobic surfaces by zinc electrodeposition on copper substrate.

2.3 Sample Characterization

X-ray diffraction (XRD) was performed on an X-ray diffractometer (XRD, D8 ADVANCE, Bruker, Germany) operating with Cu Kα radiation at a continuous scanning mode (40 kV, 40 mA, and λ = 0.15418 nm) and scanning rate of 3 °/min to characterize the crystallographic properties. Scanning electron microscope (SEM) images and energy dispersive X-ray spectroscopy (EDS) spectra were obtained on a scanning electron microscopy (SEM, S-4800, Hitachi, Japan) to reveal the micro/nanostructure morphology and chemical composition of the surfaces. X-ray photoelectron spectra (XPS, Model PHI 5300, Physical Electronics, USA), using 250 W Mg K (λ = 0.9891 nm) X-ray as the excitation source, were collected in a constant analyzer energy mode at a chamber pressure of 10^{-7} Pa and pass energy of 44.75 at 0.1 eV/step. The binding energy of carbon (284.6 eV) was used as the reference. Water contact angles (WCA) were measured with a contact anglemeter (FTÅ 200, Data physics Inc, USA) at room temperature. Water droplet (about 8 μL) was dropped carefully onto the surface, and the values reported are averages of five measurements made on different positions of the sample surface. The accuracy of CA value was ±2 °. WCA images were captured by the video and measured using a tangent algorithm due to the gravity of the droplet, which has been analyzed in detail in our previous paper.[39]

2.4 Corrosion resistance

Potentiodynamic polarization curves were used to evaluate and compare the corrosion resistance of the bare copper and superhydrophobic sample. They were recorded in a classical three electrode cell in 3.0%.wt NaCl aqueous solution at room temperature using an electrochemical workstation (CorrTest CHI760E, China); the tafel plots were acquired at a scan rate of 0.2 mV/s.

2.5 Tribological properties

Tribological properties were evaluated by a UMT Universal Mechanical Tester (UMT-1, Bruker, USA), which is a leader in mechanical and Tribology Test equipment. The tribology experiments consist of uniform load and constant load. The method of constant load is used to measure the friction coefficient of the coating surface, which was conducted by a constant loading of 50 mN with a steel ball; while the method of uniform load is used to analyze the bonding strength between film and substrate, which was

operated by a load range of 1N to 10 N with a sharp diamond drill. And the moving rate of the ball and the diamond drill during the scratch process is 0.02 mm/s and the one-way scratch length is 3 mm. The relevant experimental parameters were obtained by a real-time control computer and data analysis software.

3 Results and discussion

3.1 Morphology, wettability and Chemical compositions of the superhydrophobic surfaces

In order to gain a better understanding of the principle of SHS formation, water contact angle (WCA) measurements and SEM imaging were performed. SEM images of the sample surfaces before and after treatment with nitric acid are displayed in Fig. 1a-b, respectively. While the initial copper sheet shows a relatively smooth surface (except for some nicks) with a WCA of 72±2 °, nitric acid treatment roughens the surface (presence of nubble-protrusions and island structures), leading to increased WCA to 102±2 °. The nitric acid etched copper sheet was further modified with a zinc coating through electrodepositon process at -1.35 V for 25 min. Fig. 1c exhibits the SEM image of the morphology of the deposited structures. It is obvious that some scaly sheets preferentially grow along the protuberant parts of the gully. Electrochemical deposition of a zinc coating decreases the water contact angle to 15±2 ° (Fig. 1c). The morphology of the coating is however altered significantly after annealing, converting the scaly sheets to willow-leaf-like structures and the small particles to hexagon-like-shaped zinc structures (Fig. 1d), which may because that deposited crystal recrystallized and grow during the annealing.

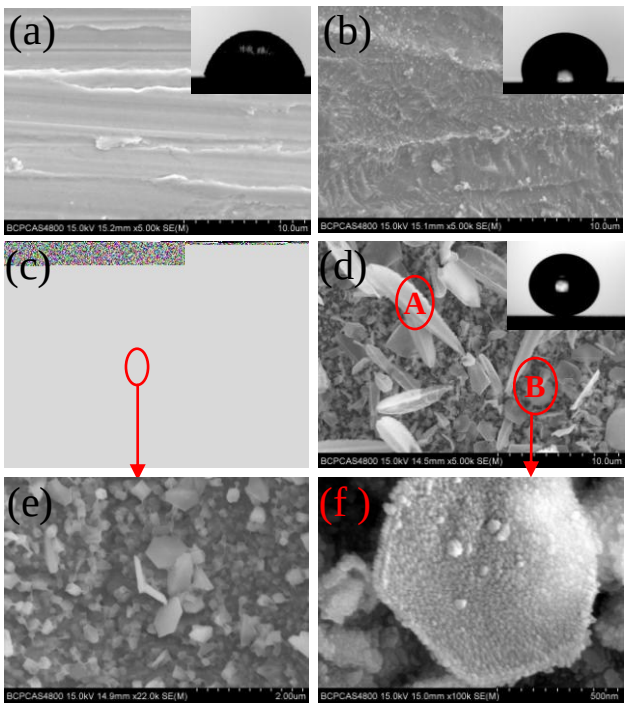

Fig. 1 SEM images and wettability of different samples: (a) untreated copper foil; (b) copper foil after treatment with HNO_3; (c) and (d) copper substrate coated with zinc film deposited by at -1.35V for 25 min before and after annealing at 190 ℃ for 60 min, respectively; (e) enlarged zone of marked by red oval with an arrow in panel (c); (f) enlarged zone of crystal B marked by red oval with an arrow in panel (d).

The surface morphology change was accompanied by a huge increase of the WCA to 170±2 °. Therefore, thermal annealing is crucial to reach superhydrophobicity of the coating. Fig. 1e and Fig. 1f display the enlarged zones of the red marked ovals in Fig. 1c and Fig. 1d, respectively. The SEM image in Fig. 1e indicates that hexagon-like-shaped crystals have already been formed in the gully during the electrodeposition; their average size is around 500 nm and then they grew bigger during the annealing process. From Fig. 1f, it can be vividly seen that countless nanoparticles with an average diameter of 30 nm bestrew on the hexagon-like-shaped crystals. It can be deduced that hierarchical micro/nanostructures are formed on the rough copper substrate so that the water droplet can easily bounce on this surface and finally roll off. In summary, the surface morphology plays a crucial role in effecting wettability of the SHSs.

In the true sense, a superhydrophobic surface should not only have a large static contact angle, but also a small slip angle. Surfaces designed in a way that water drops bounce away from them instantaneously without any adhesion have received substantial attention because of their ability to remain dry.[40, 41] Fig. 2 is a collection of images from the videos of free-falling water droplet on the micro/nano binary structured superhydrophobic sample (from Fig. 1f). The images suggest that the as-prepared SHS exhibits excellent non-sticking behavior; the water droplet rebounds upward elastically without leaving any residual traces on the surface and eventually leaves the surface within 1s with a SA of almost 0 °.

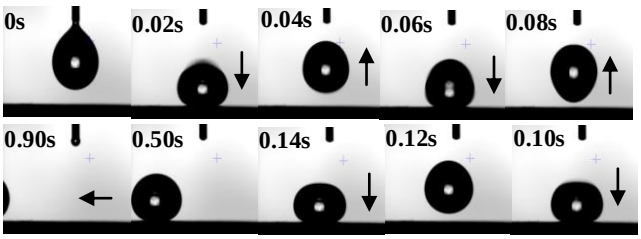

Fig. 2 Selected time sequence of snapshots of water droplets free-falling on the micro/nanobinary structured superhydrophobic sample, deposited at -1.35V for 25 min, annealed at 190 ℃ for 60 min.

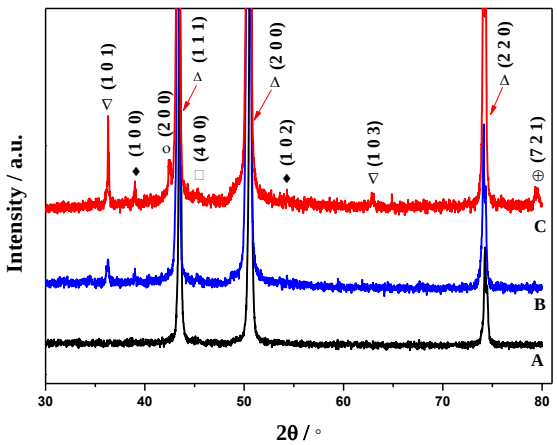

Fig. 3 XRD patterns of (A) bare copper foil, (B) and (C) the film electrodeposited at -1.35V for 25 min before and after annealing at 190 ℃ for 60 min in the air, respectively. △: Cu, ▽: ZnO, ◆: Zn, ○: CuO, □: $Zn(OH)_2$, and ⊕: Cu_5Zn_8.

It is well-known that the wetting behavior of solid surfaces is governed by both the surface morphology and the chemical composition. XRD, EDS and XPS measurements were used to

investigate the crystalline phase and chemical composition of the SHSs.

Fig. 3 shows XRD patterns in the 2θ region of 30-80° of bare copper substrate (A) and those of copper substrates coated with a zinc film, deposited at -1.35 V for 25 min, before (B) and after (C) annealing at 190 ℃ for 60 min in air. The three diffraction peaks at 2θ = 43.3°, 50.4° and 74.1° can be indexed to the face-center cubic Cu (JCPDS Card No.04-0836) corresponding to Cu(111), Cu(200) and Cu(220), respectively. After electrodeposition of the zinc coating, three new peaks at 2θ = 36.3°, 38.9°,45.3° and 54.3° ascribed to ZnO(101) (JCPDS Card No. 36-1451), Zn(100) (JCPDS Card No. 04-0831), $Zn(OH)_2$(605) (JCPDS Card No. 20-1435) and Zn(102) (JCPDS Card No. 04-0831) appeared. After annealing at 190 ℃ for 60 min in air, the diffraction peaks at 2θ = 36.3° and 38.9° became more distinct and sharper, indicating that the preferential growth of the ZnO(101) over a large substrate area during annealing process and the crystallinity increase during annealing process, too. This is in accordance with the SEM results in Fig. 1d. At the same time, two new peaks at 2θ = 62.8° and 79.5° attributed to the formation of ZnO(103) (JCPDS Card No. 36-1451) and Cu_5Zn_8 (721) alloy (JCPDS Card No. 25-1228) appeared.[42, 43] However, peaks of Zn(102), ZnO(103), $Zn(OH)_2$(605) and Cu_5Zn_8 (721) are wide in the XRD spectra, maybe they exist in small partical size. In addition, a peak of CuO (200) at 2θ = 42.2° (JCPDS Card No. 35-1258) also emerged.[44] The results indicate that hierarchical micro/nano coatings are successfully prepared by electrodeposition.

EDS analysis of the superhydrophobic coating surface displays signals due to Cu, Zn and O. Fig. S1a exhibits the EDS spectrum of the SHS surface (recorded on the crystal A marked with red oval in Fig.1d). It displays the presence of Zn and O with atomic concentrations of 88.66 and 11.34 at.%, respectively, suggesting the presence of nano-structured ZnO on the micro-structured Zn. In a similar manner, the EDS spectrum of the hexagon-like-shaped crystal B (marked by red oval in Fig. 1d) shows the presence of Cu, Zn and O with atomic concentrations of 32.90, 49.56, 17.54 at.%, respectively (Fig. S1b). The results indicate that Cu_5Zn_8 alloy was generated during the annealing step, which is in accordance with the XRD results.

XPS analysis was carried out to further determine the surface composition of the as-prepared superhydrophobic coating as shown in Fig. 4. XPS survey spectra of the zinc-coated surfaces deposited at -1.35 V for 25 min before (A) and after (B) annealing exhibit signals due to C, O, and Zn (Fig. 4a). The carbon peak is most likely due to surface contamination. Fig. 4b displays the O1s high-resolution XPS spectrum before (A) and after (B) annealing. The insets of Fig. 4b are the fitted curves of A and B, respectively. The O1s XPS spectrum of the as-prepared surface consists on a single and symmetric component, which can be typically deconvoluted into three bands at 530.2, 531.4 and 532.6 eV. The peak at 530.2 eV on the low binding side of the O1s spectrum in the curve B is attributed to O^{2-} in the Zn-O. The band at the medium binding energy (531.4 eV) of the O1s peak both in the curve A and B is associated with O_2^- ions in the zinc oxyhydroxide species ZnO(OH) that are in oxygen-deficient regions within the ZnO matrix. The component located at 532.6 eV in the curve A is usually attributed to the presence of loosely bound oxygen on the Zn surface such as adsorbed O_2 or adsorbed H_2O.[45, 46] ZnO(OH) and O_2 (or H_2O) are the main components before annealing, while ZnO and ZnO(OH) are the main components after annealing as shown in the insets of Fig. 4b.

The Cu2p high resolution XPS spectra in the range of 925-970 eV of the as-prepared sample before and after annealing at 190 ℃ for 60 min are displayed in Fig. S2. The signal is so weak that it cannot be recognized; this may be due to the presence of thick coating while CuO only formed at the Zn/Cu interface, which is beyond the detection thickness of the XPS.

The Zn2p high resolution XPS spectra of the zinc-coated substrate before and after annealing are shown in Fig. 4c and can be deconvoluted into bands at 1021.8 eV (Zn $2p_{3/2}$) and 1045.0 eV (Zn $2p_{1/2}$) before annealing. After annealing, the bands slightly shift to 1021.1 eV and 1044.2 eV. The doublet peak energy separation in both cases is 23.2 and 23.1 eV, which is consistent with the standard separation of 23.1 eV corresponding to Zn^{2+}.[47]

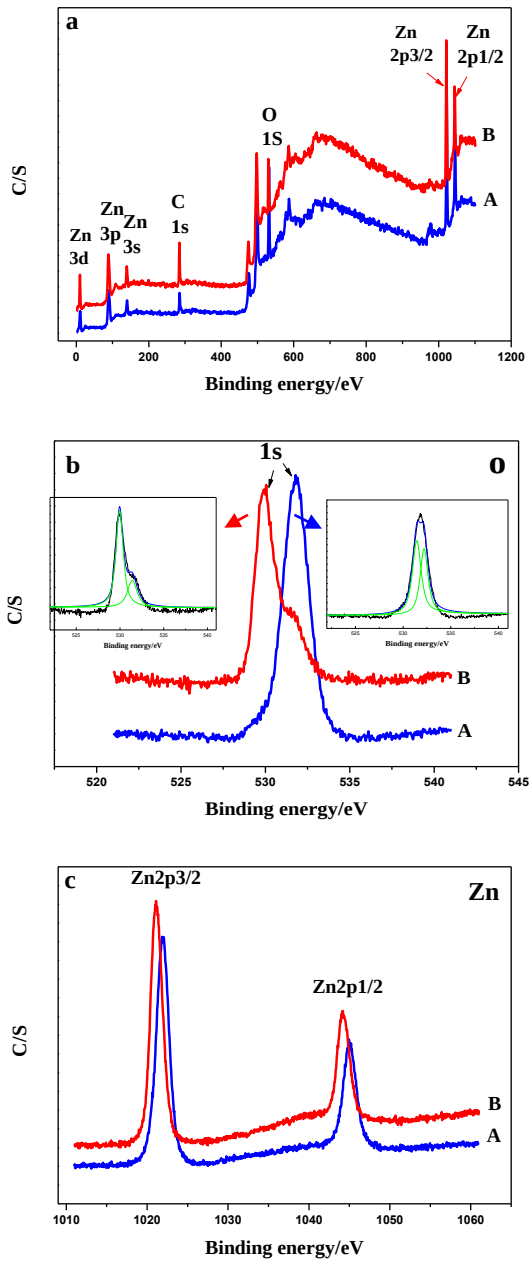

Fig. 4 XPS spectra of the samples before (A) and after (B) annealing at 190 ℃ for 60 min: (a) survey, (b) O1s, and (c) Zn2p high resolution spectra. The insets of (b) are the fitted curves of (A) and (B), respectively.

3.2 The effect of various experiment parameters

The effects of deposition potential, concentration of zinc ion (CZI), deposition time, annealing temperature and annealing time on the contact angle were studied in detail.

It is well known that the deposition potential can greatly influence the nucleation pattern of the crystal and dynamics of the coating growth, which can further effect the composition and morphology of the coating. Thus, cyclic voltammetry (CV) was carried out at different CZI in order to choose the optimum deposition potential. As shown in Fig. S3, reduction peak shifts to more negative and the position of the oxidation peak shifts to more positive with the increase of CZI. Moreover, the oxidation and reduction currents also gradually increase with the increase of CZI. A potential of -1.35 V is considered as the optimum deposition potential as more negative deposition potentials resulted in the simultaneous reduction of water and formation of bubbles. Furthermore, partially reduced Zn falls off from the copper substrate into the solution, and as a result that the surface may become very uneven and thus have a bad effect on the wetting properties. Fig.S4 revealed the curve of current with the deposition time deposited at -1.35V. It can be seen that the current increased slightly during the electrodeposition process, but fluctuations emerged at about 440s and 1060s, which may because of the diffusion delay of the zinc ions.

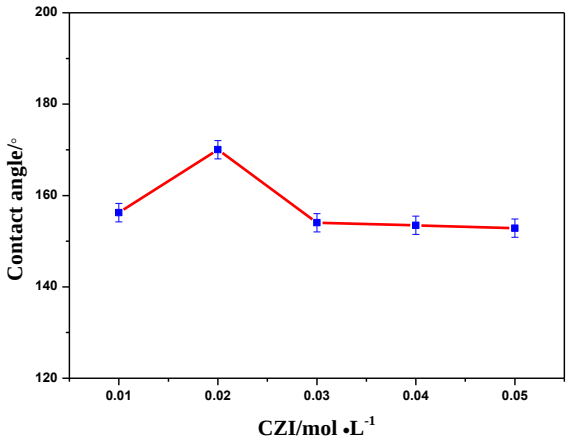

Fig. 5 Water contact angle variation with different CZI of the coating electrodeposited at -1.35 V for 25 min.

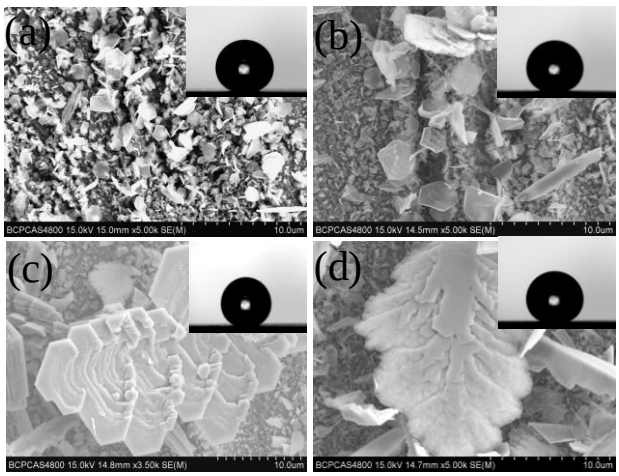

Fig. 6 SEM images and wettability of the coatings electrodeposited at -1.35 V for 25 min for different CZI: (a) 0.01 mol/L, (b) 0.03 mol/L, (c) 0.04 mol/L, (d) 0.05 mol/L, while other conditions kept constant. The samples were annealed at 190 ℃ for 60 min in air.

In order to better understand the effect of CZI on the surface wettability as well as on the coating morphology, WCAs and SEM images were used. Fig.5 depicts the variation of the WCA as a function of CZI for zinc-coated copper substrate, deposited at -1.35 V for 25 min after annealing at 190 ℃ for 60 min. The results indicate that the WCAs increase from 156±2 ° to 170±2 ° with the increase of CZI from 0.01 mol/L up to 0.02 mol/L and decrease to 154±2 °, 153±2 ° and 152±2 ° respectively for higher zinc concentrations from 0.02 mol/L to 0.05 mol/L. Evidently, 0.02 mol/L can be regarded as the optimal concentration with a WCA as high as 170±2 °.

The results suggest that the CZI plays a vital role in tailoring the morphology of the zinc films, since the crystal shape change with the increase of CZI (Fig. 6). At low CZI (0.01 mol/L), the surface is covered by lamellar crystals with typical regular hexagon and irregular hexagon morphology as well as other anomalous granulate nanostructures, which intricately arrange on the whole coating surface. When the CZI increases to 0.03mol/L, numerous flaky crystals accumulated and grow to the tower-shaped crystals along with some hexagon-like structures. The size of the tower-shaped crystals increases to several micrometers, below which are some small slice crystals with nanoscale features (Fig. 6b). In Fig. 6c are displayed the petaloid-like structures of the coating film deposited at -1.35 V from 0.04mol/L zinc ion aqueous solution. Similarly in Fig. 6d are exhibited the leaf-like crystals with an average size of 10 microns produced at CZI of 0.05mol/L. Higher CZI resulted in slower forming rate of crystal nucleus and therefore bulky crystal may be more likely to developing, which is agree with the surface topography in the Fig.6a-d. Moreover, diverse preferred orientation of the crystal growth during the process of electrodeposition may appear with the increase of CZI, which may bring about the diversification of the coating morphology.

The influence of the deposition time, annealing temperature and annealing time on the wetting properties of the zinc coating were investigated. Fig.S5a displays the WCAs of the samples deposited at -1.35V from 0.02mol/L zinc ion solution for different times, followed by annealing at 190 ℃ for 60 min in the air. It can be seen that the superhydrophobicity (WCA>150 °) was reached for electrolysis times higher than 15 min. As the time is further prolonged to 25 min, a maximum value of contact angle of 170±2 ° and a rolling angle of almost 0 ° were achieved. However, as the electrolysis time was further extended to 35 min, the WCA decreases. The reason is that it takes several minutes to form a closely packed coating on the surface, but when the time is further increased to 35 min, the coating becomes so thick that it weakens the effect of micro/nano features on the superhydrophobic property.

Fig.S5b shows the relationship between WCAs and annealing temperature for zinc films prepared at -1.35 V from 0.02 mol/L zinc ion solution for 25 min. It is noted that when annealing temperature is lower than 190 ℃, it is too low to form willow-leaf-like structures quickly to change the surface morphology. Once the annealing temperature is higher than 190 ℃, the surface morphology is destroyed and thus the superhydrophobicity decreases. It may because that atomic activity and crystal growth speed and direction varies under different annealing temperature, and thus present different crystal and surface morphology, which cause various hydrophobic. [42] The results indicate that the best results were obtained for samples annealed at 190 ℃.

The effect of the annealing time on the wetting properties was further examined. Fig.S5c depicts the WCA of the samples prepared at -1.35 V from 0.02 mol/L zinc ion solution for 25 min and annealed at 190 ℃ for various times. It is obvious that for all annealing times, superhydrophobicity was achieved although the highest WCA was recorded for 60 min. However, it is demonstrated that when the

annealing time is shorter than 60 min, crystalline Zn, ZnO, CuO and Cu_5Zn_8 generated are not enough to form suitable micro/nano binary structure. When the annealing time is longer than 60 min, it would cause more water removal from $Zn(OH)_2$ or Zn(O)(OH) to form ZnO as well as more ZnO oxidized from Zn and too many crystals will stuff the gap in rough copper substrate, and the inappropriate composition ratio would also decrease superhydrophobicity of the SHSs.

The results above demonstrate that the optimal superhydrophobic surface with a WCA as high as 170±2 ° and a SA of almost 0 ° is obtained by electrodeposition from 0.02 mol /L zinc ion solution for 25 min and annealed at 190 ℃ for 60 min.

3.3 Anticorrosion properties

The corrosion behavior of the bare copper substrate and the as-prepared superhydrophobic surface was investigated by potentiodynamic polarization tests in NaCl aqueous solution (3.0 wt. %) at a scanning rate of 0.2 mV/s (Fig.7). The corrosion potential (Ecorr), corrosion current density (Icorr) and corrosion rate are given in Table 1 using the Tafel extrapolation from the potentiodynamic polarization curves. The corrosion potential (E_{corr}/V) and the corrosion current intensity (I_{corr}/A cm^{-2}) of the bare copper sheet are about -0.2 V and 7.64 $\times10^{-8}$A/cm^2, respectively. The E_{corr} and I_{corr} of the copper substrate coated with superhydrophobic zinc film are about -0.24 V and 6.65$\times10^{-10}$ A/cm^2. In spite of the slightly shift to more negative of the superhydrophobic surface, the I_{corr} of the superhydrophobic surface is approximately 1/100 of the bare copper substrate.[6, 48] The superhydrophobic surface also exhibits very low corrosion rate, a surprising almost 133-fold decrease from the bare copper. The lower corrosion current intensity corresponds to better corrosion resistance. The results suggest that the superhydrophobic surface had better anticorrosive properties than the bare copper substrate, which may be attributed to the superhydrophobicity of the deposited coating.

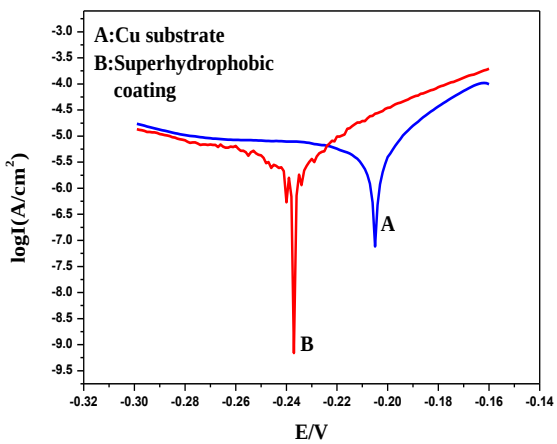

Fig. 7 Tafel polarization plots of bare copper sheet and the superhydrophobic surface in 3.0 wt.% NaCl solution at a scanning rate of 0.2 mV/s.

Table 1 Corrosion potential (Ecorr), corrosion current (Icorr) and corrosion rate of the bare Cu and superhydrophobic surface

Sample	E_{corr}(V)	I_{corr}(A/cm^2)	Corrosion rate (mm/a)
Bare Cu substrate	-0.20V	7.64×10^{-8}	9.61×10^{-7}
Superhydrophobic surface	-0.24V	6.65×10^{-10}	7.20×10^{-9}

As described in Fig. 1d, the superhydrophobic surface consists of microscale willow-like structures and small slices of hexagon covered by countless nanoscale grains, which can easily trap the air within the gaps between the hierarchical structures and form an air pocket. Furthermore, the effect of the capillary force cannot be ignored, which also contributes to the convex surface between the interface of the liquid and air. In this case, Cl^- can hardly reach the copper substrate to penetrate into the surface because of the presence of air bag and capillary force,[49] so the trapped air can serve as an effective barrier to keep corrosive media from reaching the surface and prevents the metal surface underneath from further corrosion.

In addition, the sample still keep superhydrophobic after buried in the soil at room temperature for a month, indicating that the superhydrophobic surface shows good anti-corrosion to the soil, which provides more possiblities for wider practical applications.

3.4 Chemical stability and durability

With a view to the real applications, environmental stability and durability was still the primary matter to limit the applications of superhydrophobic surfaces. The superhydrophobicity of the sample is further tested at different time intervals upon storage in ambient atmosphere to verify its environmental stability and durability. After eight months of storage in air, the values of the WCA and SA remained essentially constant, indicating that the superhydrophobicity of the hierarchical structures and chemical components were stable in air and thus exhibit long-term stability and durability, which can be seen in the AV_1 and AV_2 of the supporting information name as videos of the superhydrophobic surface tested at different time intervals .

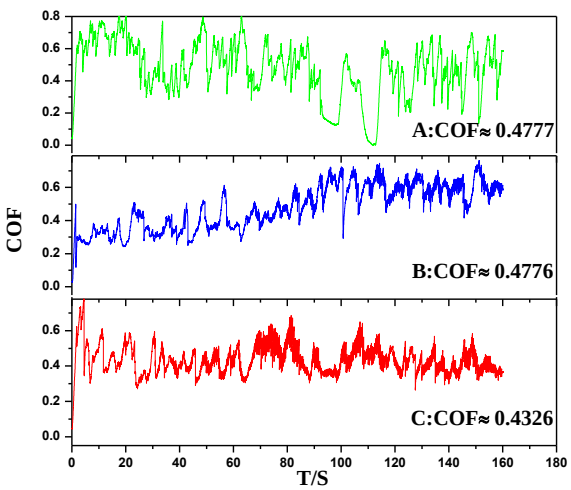

Fig. 8 Friction coefficient curves under a constant load of 50 mN: (A) copper substrate, Zn coating electrodeposited at -1.35 V for 25 min before (B) and after (C) annealing at 190 ℃ for 60 min.

3.5 Tribological properties

Constant load method was used in the scratch test to study the micro-tribological properties of the as-prepared samples. [50,51]Fig. 8 shows friction coefficient curves of different samples under a constant load of 50 mN. It can be seen from curve A that the average friction coefficient of the bare copper substrate is 0.4777 and it fluctuates obviously with the passage time. However, the friction coefficient only slightly decreased after coating (without annealing) with an average value of 0.4776 and increased gradually in the

process, as displayed in curve B. This may be due to the low stability of the non annealed film, which is just loosely arranged on the surface of the copper substrate and can be easily damaged by the sliding ball. Interestingly, the average friction coefficient decreased to 0.4326 after sample annealing at 190 ℃ for 60 min. Furthermore, the curve is relatively stable compared to curves A and B, indicating that the superhydrophobic coating reduces the friction coefficient and improves the tribological properties under the micro-load conditions.

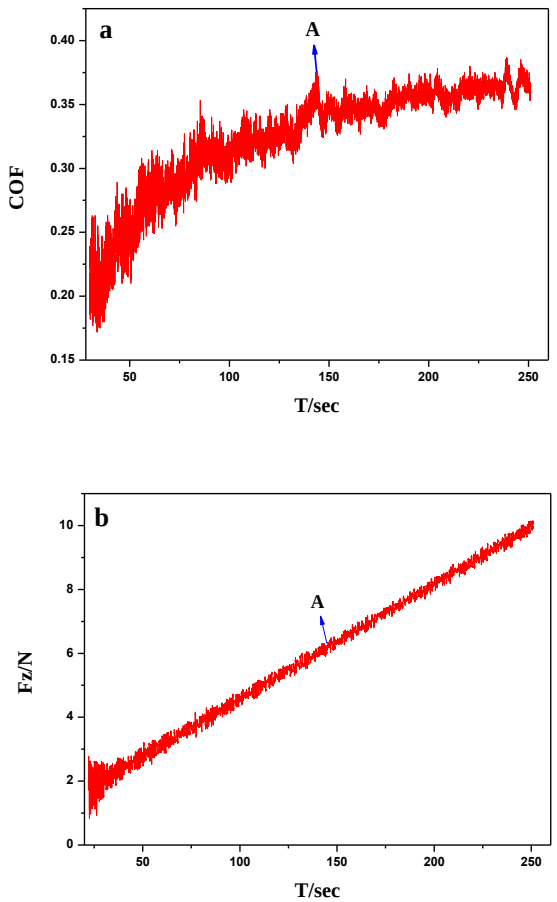

Fig. 9 Curves of Friction coefficient (a) and the uniform load (b) of the sample with the load time.

Uniform load was used in the scratch test to analyze the bonding strength between film and substrate, and the combined intensity value was evaluated by the corresponding critical load when the coating completely peeled off from the substrate surface. Fig. 9a is the curve of the friction coefficient with change of the loading time. It can be seen that the friction coefficient tends to relatively balance around the protuberant A after a slow rise with the passage of loading time, indicating that the coating was completely destroyed by the scratch around the protuberant A at the time of 144 s and since then the part of the scratch walked were the substrate, that is to say the load of protuberant A is the critical load. Fig. 9b shows the uniform variation of the load with the loading time. Compared with Fig. 9a and Fig. 9b we can infer that the load of protuberant A is about 6N, which exhibits good binding ability. Since the types of crystal structure and atomic radius of Cu atom are similar with that of Zn atom, it is easy for them to form alloy or stable solid solution structure, which often used as transition layers to enhance the binding force of related coating on the substrate, besides, formation of the intermetallic compound can enhance the affinity of substrate and the coating.

3.6 Super-buoyancy force

It is well-known that the super buoyancy force is a highly important parameter for the practical application of materials on water. In nature, water striders are kinds of insects that can stand and walk freely on a water surface using their water resistant legs. This finding may help us to design and fabricate novel drag-reducing and fastpropulsion aquatic or air devices. Copper plate sized 1.0 cm×1.0 cm×0.01cm was treated the same as the above method. When the superhydrophobic sample was laid down on to the water, it floats on the surface of the water. Moreover, the sample can keep the floating state for several months without sinking. This clearly indicates that the film has a good flotative property as shown in Fig. 10. The trapped air film surrounding the copper outer surface provides additional displaced volume of water, and prevent the sample from being wetted by water, thus results in super buoyancy force. Though application of this technology to full-sized super-floating and drag reducing aquatic devices is difficult, these novel method will find their small-scale applications in fields such as aquatic robots, environmental surveillance, and microfluidity as well as for other various potential applications. [52]

Fig. 10 Optical image of the superhydrophobic sample floating on the water.

4 Theoretical growth mechanism

On the basis of the surface structure and composition characteristics above, the corresponding growth mechanism of the special structure can be considered as the following processes. Firstly, when voltage was applied to the three-electrode system, H_2O in the system can capture electrons to form H_2 and OH^- and OH^- combined with Zn^{2+} to produce $Zn(OH)_2$. Besides, zinc ions around the working electrode are reduced to pure Zn and discharge at the same time, therefore, a metals - ion deficient layer (MIDL) with variable thickness was formed around the substrate due to varying degrees of the discharge induction, and zinc ions preferentially discharged and deposited in the projections of the substrate during subsequent electrodeposition meanwhile coating growth was inhibited in the grooves of the substrate (Fig. 1c). Localized discharge of metal ions can further contributed to surface roughening with the electrodeposition time (Scheme 2). It is noted that electric field can indirectly affect the local environment of the three electrode system, which may change the deposited structure and make the coating be mingled with oxides and hydroxides.

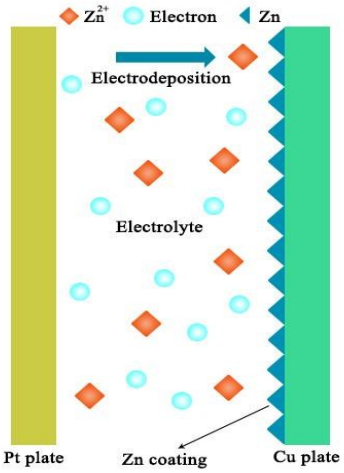

Scheme 2 Schematic diagram of the electrodeposition process.

Increasing the CZI from 0.01 to 0.05mol/L induces a change of the surface morphology as well as the crystal size, as shown in Fig. 6a-d. The crystal shape was altered from haphazardly arranged regular and irregular hexagon to willow-leaf-like structure and then to scaly pieces and tower-like and next to petaloid-like and finally to leaf topology. When the CZI is lower than 0.02mol/L or the deposition time is shorter than 25 min, Zn generated from electroposition is not enough to form suitable micro/nano binary structures. Otherwise, the crystals grow so fast and so much that they obstructed the gap in rough copper substrate, leading to non superhydrophobic surfaces. Secondly, latter in the process of annealing, Zn generated in the reduction comes into the crystal Cu lattices or interstices among them to form Cu_5Zn_8, causing crystal copper defects. Therefore, a Zn-depleted boundary layer was formed in the vicinity of the interface and the rapid decrease of the Zn concentration further changes the local equilibrium at the interface, then the reduction occurs at the sites of the copper defects continuously. Next, since oxygen dissolves in the solution and exists in the air, when annealed, the restored Zn and Cu at active lattices defects on the surface are oxidized by O_2 in air to ZnO and CuO or a mass of crystal ZnO germinate, and those generated in electrodeposition grow larger gradually on the surfaces. The annealing treatment, an industrial conventional method, changes the properties of metal surfaces. First, Annealing can promote selectively growth of certain crystal faces, resulting in lowering the surface free energy. Second, annealing of the alloy coating helps determine the crystalline phase or the alloy composition of amorphous phase. Moreover, annealing can dispel mixed gas, relax internal stress and cause changes in surface roughness and surface micro-topography through recrystallization / crystal growth, therefore, producing metallurgical changes, which promote formation of superhydrophobic surface at the right time and temperature. Another, copper substrate and coating can react with hydrophilic groups on the filter paper to form corresponding oxide during annealing to strengthen the hydrophobicity of the surface.The reaction processes can be formulated as follows:

$$2H_2O + 2e^- = H_2 + 2OH^- \quad (1)$$

$$Zn^{2+} + 2OH^- = Zn(OH)_2 \quad (2)$$

$$Zn^{2+} + 2e^- \rightarrow Zn \quad (3)$$

$$4\,Zn + O_2 + 2\,H_2O \rightarrow 4\,Zn(OH)_2 \quad (4)$$

$$Zn(OH)_2 \rightarrow ZnO + H_2O \quad (5)$$

$$2\,Cu + O_2 \rightarrow 2\,CuO \quad (6)$$

$$5\,Cu + 8\,Zn \rightarrow Cu_5Zn_8 \quad (7)$$

Two models can account theoretically for the wetting properties. One is the Wenzel model,[53] in which water drop will penetrate to the grooves of the rough surface. The other model is the Cassie-Baxter model,[54] where the superhydrophobic surface is regarded as a porous medium composed of air pockets. Furthermore, the CA change could be theoretically understood by the Cassie-Baxter equation:

$$\cos\theta = f_{sl}\,(1 + \cos\theta_0) - 1 \quad (8)$$

Where θ and θ_0 represent the WCA on a rough surface and flat surface, respectively; f_{sl} is the fractional interfacial areas of solid/water on the surface, so $(1\text{-}f_{sl})$ is the fractional areas of air/water. The value of θ_0 (72 ± 2 °) of smooth surface is almost changeless. Therefore, the larger or smaller surface roughness would increase f_{sl} and lead to the decrease in WCA (θ, 170 ± 2 °). But for the superhydrophobic surface, the trapped air can reduce the f_{sl} between a water droplet and solid surface and consequently, the hydrophobicity of the surface is dramatically enhanced, and then a high contact angle and low sliding angle are obtained.

According to equation 8, the value of f_{sl} of the superhydrophobic surface is estimated to be 0.0093, which means that the air occupies about 99.07% of the contact area between the water droplet and the composite surface. Thus, the water drops cannot penetrate into the grooves, but rather are suspended on the micro/nanostructured surface. The drops can hardly stick to the surface and will roll off quite easily from the surface with a slight inclination, even a slight vibration.

5 Conclusion

In summary, superhydrophobic surfaces with willow-leaf-like and regular hexagon structures were fabricated by an electrodeposition process without organic modification with low surface energy materials. The wettability, chemical composition, surface topography, tribological properties, chemical stability and durability, corrosion resistance and self-cleaning of the as-prepared superhydrophobic surface were evaluated. The optimal conditions and the formation mechanism of the superhydrophobic surfaces were also studied. Non-sticking behavior has been demonstrated. Excessive electrodeposition and voltage can change the micro/nano willow-leaf-like and hexagon-like structures of the coating and then decrease its superhydrophobicity. It is believed that the facile, low-cost and time-saving method would offer an effective strategy and promising industrial applications for fabricating SHSs on various metallic materials.

Acknowledgments

We gratefully acknowledge the National Natural Science Foundation of China (No. 21271027) and Bruker (Beijing) Scientific Technology Co., Ltd. for their support of this work.

Notes and references

[a] School of Chemistry, Beijing Institute of Technology, Beijing 100081, P.R. China.

[b] Institut de Recherche Interdisciplinaire (IRI, USR CNRS 3078), Université Lille1, Parc de la Haute Borne, 50 Avenue de Halley, BP 70478, 59658 Villeneuve d'Ascq, France

† Electronic Supplementary Information (ESI) available: [EDS spectrum of the interceptions of crystal A and B marked with red oval in Fig.1d. Cu2p high resolution XPS spectra of the zinc film electrodeposited at -1.35V for 25 min before (A) and after (B) annealing at 190 ℃ for 60 min in atmosphere. WCAs of the as-prepared surfaces at: (a) different deposition times at -1.35 V and annealed at 190 ℃ for 60 min, (b) different annealing temperatures for 60 min, (c) different annealing times at 190 ℃. Videos of the superhydrophobicity of the SHSs tested at different time intervals].
See DOI: 10.1039/b000000x/

1 F. Sinapi, S. Julien, D. Auguste, L. Hevesi, J. Delhalle and Z. Mekhalif, *Electrochim. Acta*, 2008, **53**, 4228.
2 Y. Huang, D. K. Sarkar, D. Gallant and X. G. Chen, *Appl. Surf. Sci.*, 2013, **282**, 689.
3 Z. Z. Zhang, X. T. Zhu, J. Yang, X. H. Xu, X. H. Men and X. Y. Zhou, *Appl. Phys. A*, 2012, **108**, 601.
4 S. J. Yuan, S. O. Pehkonen, B. Liang, Y. P. Ting, K. G. Neoh and E. T. Kang, *Corros. Sci.*, 2011, **53**, 2738.
5 H. Liu, S. Szunerits, W. Xu and R. Boukherroub, *ACS Appl. Mater. Interfaces*, 2009, **1**, 1150.
6 A. M. A. Mohamed, A. M. Abdullah and N. A. Younan, *Arabian J. Chem.*, 2014, http://dx.doi.org/10.1016/j.arabjc.2014.03.006.
7 J. P. Liu, X. T. Huang, Y. Y. Li, Z. K. Li, Q. B. Chi and G. Y. Li, *Solid State Sci.*, 2008, **10**, 1568.
8 Q. M. Pan, H. Z. Jin and H. Wang, *Nanotechnology*, 2007, **18**, 355605.
9 Y. Li, W. Z. Jia, Y. Y. Song and X. H. Xia, *Chem. Mater.*, 2007, **19**, 5758.
10 N. J. Shirtcliffe, G. McHale, M. I. Newton and C. C. Perry, *Langmuir*, 2005, **21**, 937.
11 N. J. Shirtcliffe, G. McHale, M. I. Newton, G. Chabrol and C. C. Perry, *Adv. Mater.*, 2004, **16**, 1929.
12 N. J. Shirtcliffe, G. McHale, M. I. Newton and Y. Zhang, *ACS Appl. Mater. Interfaces*, 2009, **1**, 1316.
13 W. Li and Z. Kang, *Surf. Coat. Technol.*, 2014, **253**, 205.
14 L. Mishchenko, B. Hatton, V. Bahadur, J. A. Taylor, T. Krupenkin and J. Aizenberg, *ACS Nano*, 2010, **4**, 7699.
15 D. Tian, X. F Zhang, X. Wang, J. Zhai and L. Jiang, Phys. Chem. Chem. Phys., 2011, 13, 14606.
16 T. Sun, L. Feng, X. Gao and L. Jiang, *Acc. Chem. Res.*, 2005, **38**, 644.
17 F. Chen, D. S. Zhang, Q. Yang, J. L. Yong, G. Q. Du, J. H. Si, F. Yun and X. Hou, *ACS Appl. Mater. Interfaces*, 2013, **5**, 6777.
18 T. Darmanin, E. Taffin de Givenchy, S. Amigoni and F. Guittard, *Adv. Mater.*, 2013, **25**, 1378.
19 Y. Y. Yan, N. Gao and W. Barthlott, *Adv. Colloid Interface Sci.*, 2011, **169**, 80.
20 X. M. Li, D. Reinhoudt and M. Crego-Calama, *Chem. Soc. Rev.*, 2007, **36**, 1350.
21 X. Zhang, F. Shi, J. Niu, Y. Jiang and Z. Wang, *J. Mater. Chem.*, 2008, **18**, 621.
22 P. Ragesh, V. A. Ganesh, S. V. Nair and A. S. Nair, *J. Mater. Chem. A*, 2014, **2**, 14773.
23 Z. Guo, W. Liu and B.-L. Su, *J. Colloid Interface Sci.*, 2011, **353**, 335.
24 C. Neto, K. R. Joseph and W. R. Brant, Phys. Chem. Chem. Phys., 2009, 11, 9537.
25 B. N. Sahoo and B. Kandasubramanian, *RSC Adv.*, 2014, **4**, 22053.
26 G. Caputo, R. Cingolani, P. D. Cozzoli and A. Athanassiou, Phys. Chem. Chem. Phys., 2009, 11, 3692.
27 P. Roach, N. J. Shirtcliffe and M. I. Newton, *Soft Matter*, 2008, **4**, 224.
28 Z. Chen, L. Hao, A. Chen, Q. Song and C. A. Chen, *Electrochim. Acta*, 2012, **59**, 168.
29 F. Su, K. Yao, C. Liu and P. Huang, *J. Electrochem. Soc.*, 2013, **160**, D593.
30 Y. Zhang, Y. Chen, L. Shi, J. Li and Z. Guo, *J. Mater. Chem.*, 2012, **22**, 799.
31 B. P. Binks and A. Rocher, Phys. Chem. Chem. Phys., 2010, 12, 9169.
32 N. Verplanck, Y. Coffinier, V. Thomy and R. Boukherroub, *Nanoscale Res. Lett.*, 2007, **2**, 577.
33 X. F. Gao and L. Jiang, *Nature* 2004, **432**, 36.
34 D. Quéré, *Rep. Prog. Phys.*, 2005, **68**, 2495.
35 W. G. Xu, T. Ning, X. Yang and S. X. Lu, *Appl. Surf. Sci.*, 2011, **257**, 4801.
36 X. F. Shi, S. X. Lu and W. G. Xu, *Mater. Chem. Phys.*, 2012, **134**, 657.
37 T. Ning, W. G. Xu and S. X. Lu, *Appl. Surf. Sci.*, 2011, **258**, 1359.
38 J. X. Wang, S. X. Lu, W. G. Xu and Y. Zhang, *RSC Adv.*, 2014, **4**, 39197.
39 N. Zhang, S. X. Lu, W.G. Xu and Y. Zhang, *New J. Chem.*, 2014, **38**, 4534.
40 F. Wang, S. Lei, C. Li, J. Ou, M. Xue and W. Li, *Ind. Eng. Chem. Res.*, 2014, **53**, 7141.
41 F. H. Su and K. Yao, *ACS Appl. Mater. Interfaces*, 2014, **6**, 8762.
42 J. Wang, C. Lin and C. M. Chen, *Scr. Mater.*, 2011, **64**, 633.
43 M. Farbod and A. Mohammadian, *Intermetallics*, 2014, **45**, 1.
44 Z. X. She, Q. Li, Z. W. Wang, L. Q. Li, F. N. Chen and J. C. Zhou, *Chem. Eng. J.*, 2013, **228**, 415.
45 E. De la Rosa, S. Sepulveda-Guzman, B. Reeja-Jayan, P. S. A. Torres, N. Elizondo and M. Jose Yacaman, *J. Phys. Chem. C*, 2007, **111**, 8489.
46 P. S. Kumar, J. Sundaramurthy, D. Mangalaraj, D. Nataraj, D. Rajarathnamd and M. P. Srinivasan, *J. Colloid Interface Sci.*, 2011, **363**, 51.
47 N. L. Tarwal, A. V. Rajgure, A. I. Inamdar, R. S. Devan, I. Y. Kim, S. S. Suryavanshi, Y. R. Ma, J. H. Kim and P. S. Patil, *Sens. Actuators A*, 2013, **199**, 67.
48 Z. X. She, Q. Li, Z. W. Wang, L. Q. Li, F. N. Chen, J. C. Zhou, *ACS Appl. Mater. Interfaces*, 2012, 4, 4348
49 T. Liu, Y. Yin, S. Chen, X. Chang and S. Cheng, *Electrochim. Acta*, 2007, **52**, 3709.
50 T. Verho, C. Bower , P. Andrew, S. Franssila, O. Ikkala and R. H. A. Ras, *Adv Mater*, 2011, **23**, 673.
51 J. P. Zhang, B. C. Li, L.Wu and A. Q. Wang, *Chem. Commun.* 2013, **49**, 11509.
52 Q. Pan and M. Wang, *ACS Appl. Mater. Interfaces*, 2009, **1**, 420.
53 R. N. Wenzel, *Ind. Eng. Chem.*, 1936, **28**, 988.
54 A. B. D. Cassie and S. Baxter, *Trans. Faraday Soc.*, 1944, **40**, 546.